IEEE Access
Multidisciplinary ⋮ Rapid Review ⋮ Open Access Journal

Received September 27, 2020, accepted October 12, 2020, date of publication October 22, 2020, date of current version November 2, 2020.

Digital Object Identifier 10.1109/ACCESS.2020.3032978

An Automatic Calibration Method for AVM Cameras

YUN HEE LEE[1,2], AND WHOI-YUL KIM[2], (Member, IEEE)

[1]Litbig, Seongnam 13487, South Korea
[2]Department of Electronics and Computer Engineering, Hanyang University, Seoul 04763, South Korea

Corresponding author: Whoi-Yul Kim (wykim@hanyang.ac.kr)

This work was supported in part by the Korea Evaluation Institute of Industrial Technology (KEIT) grant funded by the Korea Government (MOTIE), Road Surface Condition Detection Using Environmental and In-Vehicle Sensors, under Grant 20000293.

ABSTRACT We introduce a method for the efficient calibration of around-view-monitoring (AVM) cameras. Particularly, we introduce two situations that require calibration because of the characteristics of AVM cameras: a situation wherein cameras are shipped from the manufacturing line and another situation wherein some cameras are distorted during operation and need recalibration. In this study, the calibration method for shipped cameras is defined as the factory mode and that for recalibration is defined as the service mode. In the factory mode, two circular patterns placed at a regular distance are used to ensure the maximum accuracy while requiring minimum calibration. In the service mode, as a recalibration method, we developed a robust method that considers various environments using parallel parking lines that can be easily installed in general service centers. In the factory mode, we confirmed that the AVM-camera-calibration error was within 5.66 cm when the two circular patterns were located at a certain distance within a certain range. However, in the service mode, we achieved camera movement angle error equal to or less than 0.1° using the parking-line-detection result.

INDEX TERMS Around-view-monitoring (AVM) system, fish-eye lens camera, automatic camera calibration, parking-line detection.

I. INTRODUCTION

Recently, the automotive industry has been rapidly developing because of the increase in the number of vehicles, and the development is focused on creating systems that add to the convenience of drivers [1]–[3]. Among these systems, parking systems have been developed using ultrasonic sensors, rear cameras, around-view-monitoring (AVM) cameras, and automatic parking systems [4]–[6]. Especially, camera-based convenience systems have been developed more after their mandatory installation [1]–[6]. In this study, we focus on an AVM system, which comprises cameras in the front, rear, left, and right of the vehicle, respectively, to display the 360° view of the surroundings of the vehicle. Additionally, we focus on constructing a system that assists in parking by synthesizing images from the cameras to from a top-view image [1], [2], [8]–[13]. However, AVM cameras must be calibrated to synthesize top-view images. In AVM-camera calibration, the information regarding the mounting position and angle of the camera is calculated, following which the input image is converted into the top-view image. Generally, AVM-camera calibration involves considerable time because the system needs to know the position of the pattern and point on the image. Most calibration methods match the pattern position in an image by using the dot of the pattern at a certain position [2], [14], while some methods perform calibration by automatically finding feature points using a certain point. Additionally, some methods use the license-plate position [8], [9] and front-camera vanishing point [8]. When the initial mounting position and angle of a camera are known,there are some methods that use a lane while driving or a feature point. In this study, two calibration methods are proposed depending on the installation position and mounting angle of the camera. One is the calibration method in factory mode and the other is in service mode. Table 1 presents the comparison between the factory and service modes. As shown in the Table 1, in the factory mode, the camera-position and angle information as the initial input

The associate editor coordinating the review of this manuscript and approving it for publication was Wei Liu.

TABLE 1. Comparison between factory and service modes.

	Factory Mode	Service Mode
Initial Value	None	Yes
Area	Wide	Restricted
Ground	Poly Urethane	Various
Pattern	Circular Pattern	None

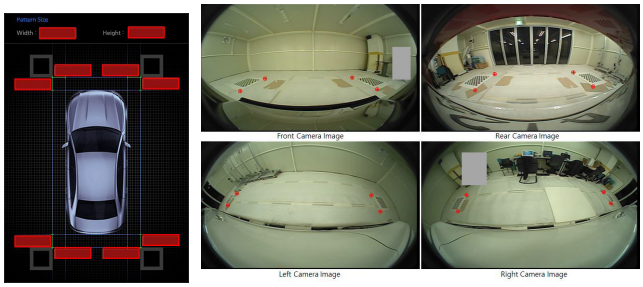

FIGURE 1. Example of a manual calibration method: (a) pattern location input and (b) image point input.

does not exist, and the calibration must be quickly and accurately performed. Additionally, calibration is performed in a garage environment, which is not as spacious and lighted as a factory floor. However, in the service mode, sufficient space is often not available. Because the camera-location and angle information, as the initial input, is known, the initial-input information can be corrected using the parking line detection result.

In an existing camera calibration method, a square pattern is placed in the area where each camera overlaps, and each distance to the vehicle is manually measured as an input and subsequently a point in the image is selected. As the calibration pattern should be observed over a certain size in the camera, it is prepared and placed in 1 m size. Moreover, extensive experience is required to measure the exact location. Figure 1 shows an example of an existing method. As shown in Fig. 1 (a), the size of the pattern located at each corner of the vehicle and the distance from the vehicle corner must be measured and used as input. Figure 1 (b) displays an example of acquiring image coordinates by clicking the edge of the pattern in each image. Accordingly, the image coordinates were obtained by manually clicking the edge of the pattern. Through this process, world and image coordinates are found, and camera calibration can be performed. If the pattern is not installed, it takes more than 30 minutes even for the skilled person to place the pattern. Even after the pattern is installed, it takes a few minutes or more because the input value must be provided. The proposed method eliminates the time to install the pattern and put input values through the automatic calibration method.

Calibration in the factory mode is performed by acquiring an image using an AVM camera as the vehicle passes between two parallel circles. In the factory environment, the cameras move in a sequence, and they are calibrated after being

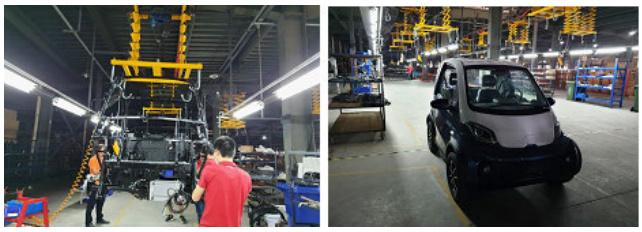

FIGURE 2. Example of factory environment.

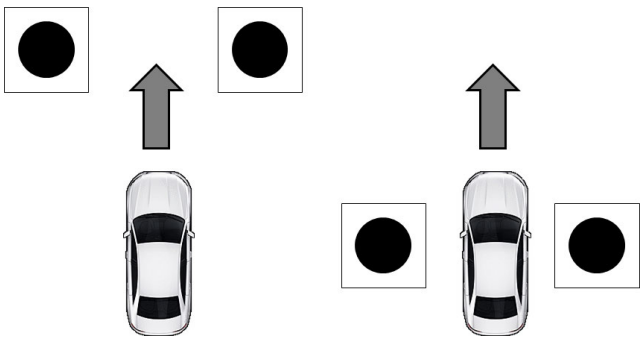

FIGURE 3. Factory-mode calibration example.

assembled. Simultaneously, because the vehicle travels along a straight line, the production may proceed quickly if the image is acquired as the vehicle continues to move instead of stopping at a certain position for a considerable time. Figure 2 depicts an example of the factory environment. Thus, in the proposed method, when we know the sizes of the two circles between whom the vehicle passes, we can calculate the vanishing point and estimate the position of both the circles and camera. Additionally, as the vehicle moves, the circles appear at various positions in the left and right cameras. Thus, one can calibrate the left and right cameras using two or more circles and, finally, calibrate the camera using the two circles that appear in the rear camera. Figure 3 depicts an example wherein the vehicle passes between two circular patterns. Figure 3 depicts the factory mode wherein camera calibration is automatically performed by passing the vehicle between two parallel circles.

Calibration in the service mode is performed using the parking line detection result. The vehicle recognizes a parking line and calculates the position and angle of the parking line. In the service mode, it is difficult to make sufficient space for the calibration pattern. However, because the previous calibration results are stored, the degree of camera movement can be calculated. Figure 4 depicts a service center; there is not adequate area for the calibration pattern, and the vehicle must be serviced within a small space.

In the service mode, calibration is performed by measuring the rotation of each AVM camera by using the position and shift of the parking line. Figure 5 depicts an example of service-mode calibration. If there exist a parking line, as depicted in Fig. 5, it is recognized and used for calibration.

FIGURE 4. Example of a service center.

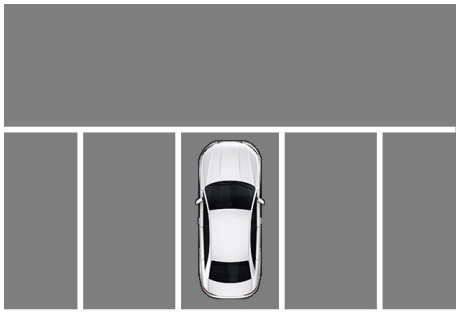

FIGURE 5. Service-mode calibration.

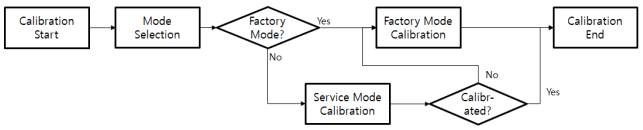

FIGURE 6. Block diagram of the proposed method.

In our study, an automatic AVM-camera-calibration method in two modes is proposed for the cases wherein there exists no information regarding the position and mounting angle of the camera and wherein the camera is distorted because of internal and external influences. Figure 6 depicts a block diagram of the proposed method. If no information exists regarding the position and mounting angle of the camera, the factory mode is used; otherwise, the service mode is used. If the information is corrected, the camera calibration is realized, and if calibration is not possible, the calibration is performed again through the factory mode.

II. FACTORY-MODE CALIBRATION

In the factory mode, one requires the position of a circular pattern and a homography matrix before performing camera calibration using the circular pattern. The proposed method detects a circular pattern using a pair of gradient vectors and calculates the homography matrix using the extracted circular pattern.

A. CIRCULAR-PATTERN DETECTION USING A PAIR OF GRADIENT VECTORS

Generally, the methods that detect a circular pattern use the circle Hough transform [15]–[17]. The proposed method employs a pair of gradient vectors to quickly detect a circular pattern by using a black pattern on a white background. In the proposed method, a Laplacian-of-Gaussian filter is applied to find the gradient vector [18]. The proposed method also confirms whether the pattern is circular because otherwise errors may occur while detecting the pattern, resulting in misrecognition of other objects as patterns upon using the gradient vectors [18]. Figure 7 depicts some example cases of misrecognition of surrounding objects as patterns. Figure 7 (a) depicts a case of misrecognizing the windshield of the vehicle and Fig. 7 (b) a case of misrecognizing a tree. To suppress misrecognition, binarization is used to verify whether the pattern is circular. The proposed method uses binarization to find the outer part of the circle by separating the circle and background parts, and to verify the pattern circularity by detecting the direction of the edge in the outer part of the circle [19]. Figure 8 depicts the result of detecting a circular pattern in an input image.

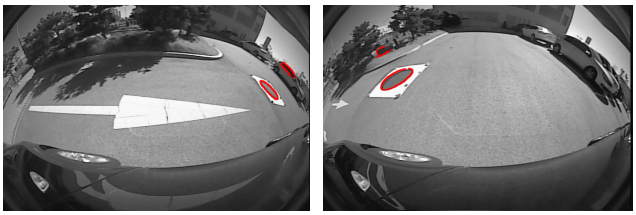

(a) (b)

FIGURE 7. Wrong circle-detection result: (a) windshield misrecognition and (b) tree misrecognition.

FIGURE 8. Circle-detection result.

As depicted in Fig. 8, because the AVM camera uses a high-distortion fisheye lens, the circular pattern appears as an ellipse in the input image. However, through binarization, the pattern circularity is verified, and thus the pattern is accurately extracted.

B. HOMOGRAPHY MATRIX USING CIRCLE DETECTION

Using the circle extracted, we can calculate a homography matrix that represents the relationship between the camera and ground. The circular pattern on the ground appears as an ellipse in the AVM camera image. Thus, the camera must be calibrated using the elliptic equations to extract a homography matrix [20]–[23]. Equations (1) and (2) represent the elliptic equations [21] as follows:

$$a_1x^2 + a_2xy + a_3y^2 + a_4x + a_5y + a_6 = 0. \quad (1)$$

$$b_1x^2 + b_2xy + b_3y^2 + b_4x + b_5y + b_6 = 0. \quad (2)$$

Upon rearranging Eqs. (1) and (2) for x and y, we obtain the following:

$$f(x, y) = a_1x^2 + (a_2y + a_4)x + (a_3y^3 + a_5y + a_6). \quad (3)$$
$$f(x, y) = b_1x^2 + (b_2y + b_4)x + (b_3y^3 + b_5y + b_6). \quad (4)$$

When Eq. (4) is reorganized with respect to y, it is expressed as follows:

$$q(r) = r_4y^4 + r_3y^3 + r_2y^2 + r_1y + r_0. \quad (5)$$

Equation (5) is expressed in the form of a Q-matrix, which is represented in Eq. (6), where y and x from Eqs. (3) and (4) can be obtained using the eigenvalue of the Q-matrix. One has

$$Q = \begin{pmatrix} 0 & 0 & 0 & -r_0/r_4 \\ 1 & 0 & 0 & -r_1/r_4 \\ 0 & 1 & 0 & -r_2/r_4 \\ 0 & 0 & 1 & -r_3/r_4 \end{pmatrix}. \quad (6)$$

Homography matrix H is decomposed as H_A (affine), H_A (projection), and H_S (scale). H_S can be ignored because scale factor is determined by the display size [23]. H_A and H_A are represented using Eq. (7) and Eq. (8), respectively, as follows:

$$H_P = \begin{pmatrix} 1 & 0 & 0 \\ 0 & 1 & 0 \\ l_1 & l_2 & l_3 \end{pmatrix}. \quad (7)$$

$$H_A = \begin{pmatrix} 1/\beta & -\alpha/\beta & 0 \\ 0 & 1 & 0 \\ 0 & 0 & 1 \end{pmatrix}. \quad (8)$$

In the elliptic equations from Eqs. (1) and (2), the points of all the circles in a plane pass through $I = (1 \quad i \quad 0)^T$ and $J = (1 \quad -i \quad 0)^T$. Additionally, is located in the vanishing line [23]. Accordingly, the point that passes through the H-matrix and the circle can be expressed as

$$HI = H_P^{-1}H_A^{-1}I = \begin{pmatrix} \beta + i\alpha \\ i \\ -l_1/l_3(\beta + i\alpha) - il_2/l_3 \end{pmatrix}. \quad (9)$$

In summary, Eq. (9) be expressed as

$$HI = \begin{pmatrix} \alpha l_3 - i\beta l_3 \\ l_3 \\ -l_2 - l_1\alpha + il_1\beta \end{pmatrix}. \quad (10)$$

If HI is defined as $z = (x \quad y \quad 1)^T$, it can be summarized as

$$z = \begin{pmatrix} xy^* \\ yy^* \\ 1y* \end{pmatrix} = \begin{pmatrix} z_1 + iz_2 \\ z_3 \\ z_4 + iz_5 \end{pmatrix}. \quad (11)$$

Using Eq.(11), α, β, and l_∞ can be expressed as

$$\alpha = z_1/z_3. \quad (12)$$
$$\beta = -z_2/z_3. \quad (13)$$
$$l_\infty = (-z_5z_3/z_2 \quad z_5z_1/z_2 - z_4 \quad z_3)^T. \quad (14)$$

When the number of circular patterns is more than two, the errors generated in the detection of each circular pattern

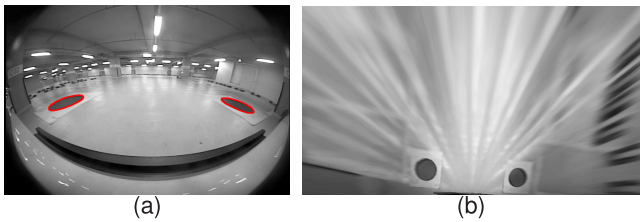

FIGURE 9. *H*-matrix-extraction result: (a) circle detection result and (b) converted image.

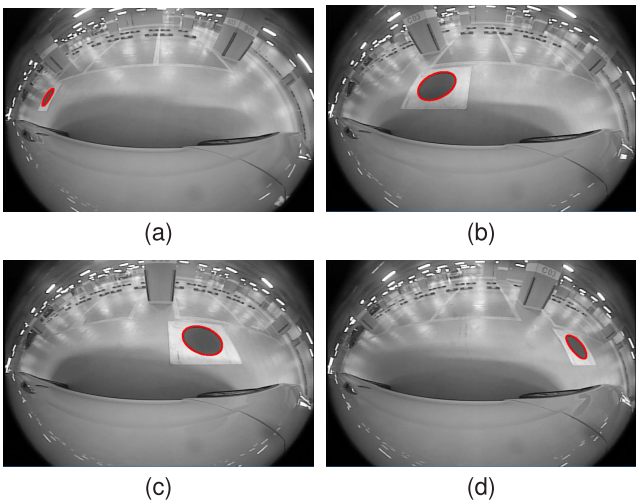

FIGURE 10. Circle-detection result in a moving picture: (a) 15th frame, (b) 23rd frame, (c) 30th frame, and (d) 40th frame.

are obtained using an H-matrix. In Eqs. (12)–(14), k denotes the number of circles, M the maximum error, and m the minimum error of the k-th circle [23]. One has

$$\varepsilon(p) = \sum_{k=2}^{n} |1 - (\frac{m_k}{M_k})^2|. \quad (15)$$

The calibration accuracy is improved by obtaining the H-matrix except for a circle with large error. Figure 9 depicts the result of transforming two circular pattern using the H-matrix.

C. HOMOGRAPHY MATRIX FROM MOVING PICTURE

Extracting an H-matrix using circular patterns from multiple images is equivalent to using multiple circular patterns in one image. Because the positions of circles are different in multiple images, the overall effect is the same as though there are multiple circular patterns in one image. Figure 10 depicts the result of extracting the same circular pattern from various images acquired by a moving camera.

As depicted in Fig. 10, because the position of the circle is different in each frame, the same method used for multiple circular patterns in one image can be employed. Equation (15) calculate the error of each circular pattern. By using the equation, an H-matrix can be obtained by excluding the image that has a significant error. Figure 11 depicts the top-view image obtained using the extracted H-matrix.

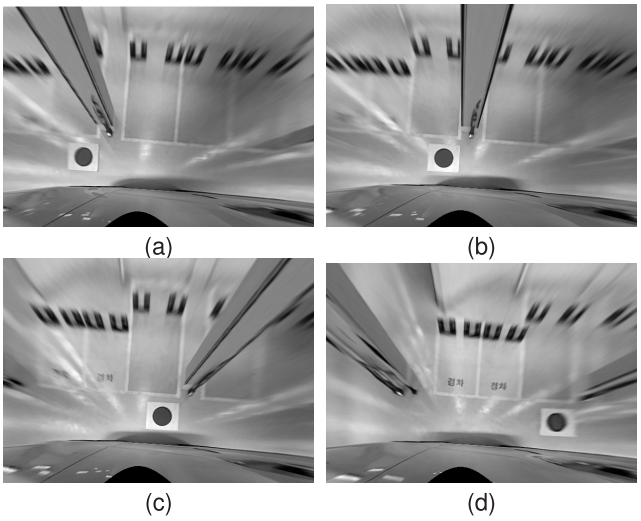

FIGURE 11. Top-view image: (a) 15th frame, (b) 23rd frame, (c) 30th frame, and (d) 40th frame.

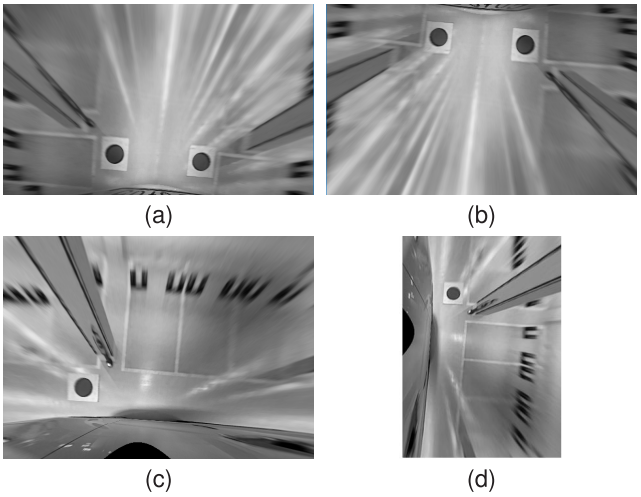

FIGURE 12. Rotated image: (a) rear-camera top-view image and (b) rotated result of (a). (c) right-camera top-view image and (d) rotated result of (c).

D. IMAGE SYNTHESIS

To generate an AVM image, the overlapping region between the original and rotated images must be synthesized. Image rotation comprises two parts: changing the mounting angle of the camera to match the vehicle-movement direction and changing the angle using line that connects the center of the circular pattern. The purpose of changing the angle to match the vehicle-movement direction is to match the vehicle-movement direction with the direction of the camera. Because the front camera image is along the direction that the camera faces, image rotation is not required. However, the rear-camera image should be rotated by 180°, right camera image by 90°, and left camera image by –90°. Figure 12 depicts the result of image rotations. Figure 12 (a) illustrates the rear camera image converted into the top-view one, and Fig. 12 (b) shows the result of rotating the image by 180°. Figure 12 (c) and (d) depicts the right camera image converted into the top-view one and shows the result of image rotation by 90°.

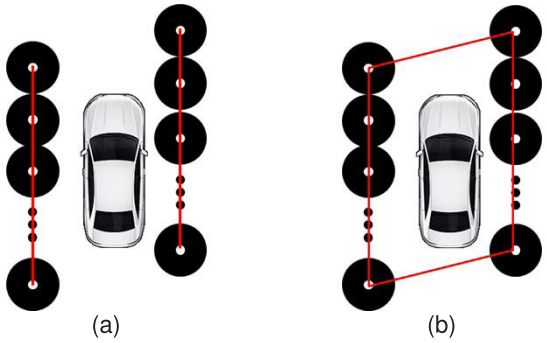

FIGURE 13. AVM-image-synthesis method using circle-detection results: (a) left and right image, and (b) front and rear image.

After rotating the direction of each camera to match the direction of the vehicle, the images also must be rotated using the line that connects the center of the circular pattern to synthesize AVM top-view images. This rotation is simultaneously performed with top-view image synthesis. To synthesize the circular pattern from the image acquired from each camera, the size and position of the circle from each camera image are used. The circle position in the top-view image generated by each camera is the same as that in the AVM image acquired at the same time t. Conversely, the position of the circular pattern in the image acquired at the t-th frame by the front camera and the position of the circular pattern in the images acquired at the t-th frame obtained by the left and right cameras have the same coordinates in the world coordinate system. Thus, the lines that connect the centers of the circles from each frame form a parallelogram because the coordinates of the center of each circle center are constant. Figure 13 depicts the parallelogram-formation process by connecting the centers of circular patterns from each image.

As depicted in Fig. 13, if the center coordinates of a circle from multiple frames obtained using the left and right cameras are connected, they are expressed as parallel lines because the vehicle moves along a straight line. The parallelism between the left and right lines is used to calculate the mean square error (MSE) and synthesize the AVM image when the MSE is within a threshold. Figure 14 depicts the result of generating an AVM composite image.

III. SERVICE-MODE CALIBRATION

Calibration in the service mode uses parking lines. The AVM camera is calibrated using a pair of parallel parking lines, which are recognized via their edges in AVM images. Additionally, the AVM camera is calibrated by measuring the changes in the parking line using their vanishing point.

A. PARKING-LINE DETECTION

The parking-line-recognition method extracts an edge from an AVM image and recognizes a line component using the Hough transform. Because parking lines have a straight-line

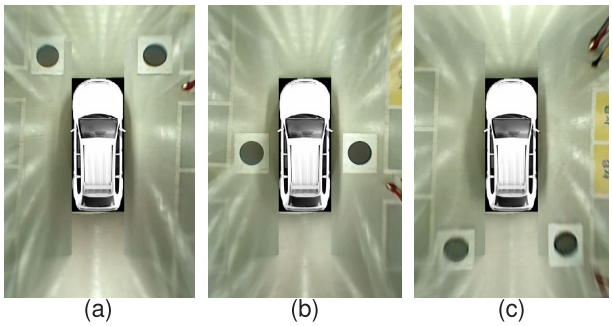

FIGURE 14. AVM-image-synthesis result: (a) 15th frame, (b) 27th frame, and (c) 40th frame.

component, the Sobel edge detector can be used to find the edge of the straight line in the AVM image. The Sobel edge detector has the advantage of reducing noise and finding the edge component, while requiring only a small amount of computation. Using the Sobel edge detector, horizontal and vertical edges are distinguished and extracted. Equations (16) and (17) represent the Sobel edge detector method to find the horizontal and vertical edges, where E_H denotes a horizontal-edge image and E_V a vertical-edge image. Additionally, I denotes the input image, x and y the image coordinates, H the image height, and W the image width [13], [24]. One has

$$\begin{aligned} E_H = & \sum_{y=1}^{H-1} \sum_{x=1}^{W-1} I(x-1, y+1) + 2I(x, y+1) \\ & + (x+1, y+1) - I(x-1, y-1) \\ & - 2I(x, y-1) - (x+1, y-1). \end{aligned} \tag{16}$$

$$\begin{aligned} E_V = & \sum_{y=1}^{H-1} \sum_{x=1}^{W-1} I(x+1, y-1) + 2I(x+1, y) \\ & + (x+1, y+1) - I(x-1, y-1) \\ & - 2I(x-1, y) - (x-1, y-1). \end{aligned} \tag{17}$$

Figure 15 depicts the edge-extraction results obtained using the Sobel edge detector. Figure 15 (b) and (c) depicts the results of finding the vertical and horizontal edges, respectively. Figure 15 (a) depicts that the front camera image is distorted; thus, it is out of order. Parking lines are recognized by applying the Hough transform to the edge-extraction results. The Hough transform processes all the linear components that pass through a point into distance and angular components from the midpoint, and this gives us an advantage in that a straight line through which the most points pass can be detected. Equation (18) represents the Hough transform, where x and y denote image coordinates, θ the slope of the straight line, and r the distance between the origin and the straight line [13], [24]. One has

$$x \cos\theta + y \sin\theta = r. \tag{18}$$

The strongest edge component can be obtained using the Hough transform by analyzing the rising and falling edges. Because the parking line has a thick line component, it has

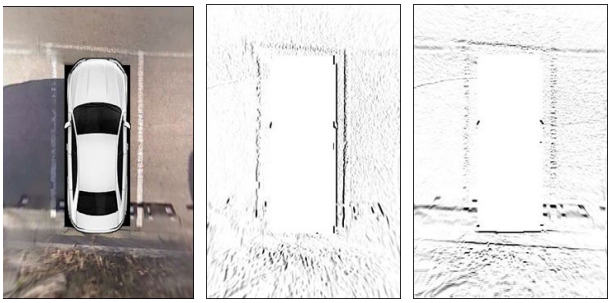

FIGURE 15. Edge-extraction result: (a) AVM image, (b) vertical-edge extraction, and (c) horizontal-edge extraction.

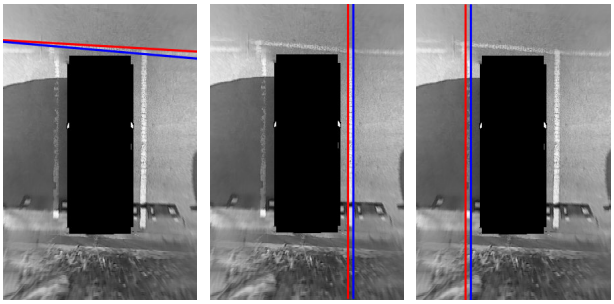

FIGURE 16. Parking-line-detection result: (a) front line, (b) right line, and (c) left line.

two components: a rising edge, which represents the intensity change from dark to bright, and a falling edge, which represents the intensity change from bright to dark. The AVM image can be corrected again using the rising and falling edges [13]. Figure 16 depicts the Hough-transformation result. The red and blue lines represent the rising and falling edges, respectively. Figure 16 (a), (b), and (c) depict the line-detection results in the front-camera, right-camera, and left-camera regions, respectively.

B. AVM CAMERA CALIBRATION

In order to calibrate the AVM camera, images obtained from each camera were divided and used. As shown in the Fig. 17, area A-D uses only the camera image at each location, but area E-H is the area where the cameras overlap.

To calibrate the AVM cameras, the images obtained from each camera are divided and used. As depicted in Fig. 17, Areas A–D are from only one image, but Areas E–H are the ones where the camera images overlap.

As depicted in Fig. 18, vanishing points are formed because the thicknesses of the left and right parking lines are different. However, if the AVM camera is satisfactorily calibrated, a vanishing point is not formed, and thus a straight line forms an angle of 90° with the center line of the vehicle.

The AVM-camera-calibration method assumes that the parking lines are parallel in the AVM image. However, if the parking lines are not parallel, a vanishing point is formed, and the angle of the camera is extracted from it. The

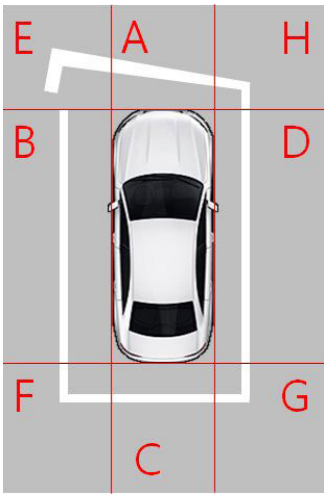

FIGURE 17. AVM-image section.

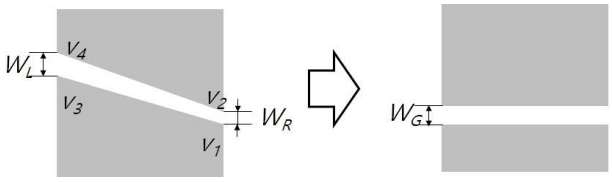

FIGURE 18. AVM-camera-calibration method in the service mode.

camera-movement angle can be measured using the location of the vanishing point. Equations (19) and (20) show the relationship between the vanishing point and camera-movement angle [13]. One has

$$\theta = \cos^{-1}(\bar{v} \cdot v_u). \tag{19}$$

$$v_u = \bar{v} \times v_\infty., \tag{20}$$

where v denotes the vanishing point; notably, $\bar{v} = v/||v||$ and $v_\infty = [0 \quad 1 \quad 0]^T$. The AVM camera can be calibrated using the angle θ obtained from the following:

$$R = (\cos\theta)I + (\sin\theta)[v_u]_\times + (1 - \cos\theta)(v_u \otimes v_u). \tag{21}$$

When the homography matrix H is derived using the obtained R matrix, it appears as follows. Here, l denotes a parking line, and l' denotes a parking line in which the vanishing point approaches infinity [13]. One has

$$l' = H^{-T}l = (KRK^{-1})^{-T}l. \tag{22}$$

The relationship between the image and world coordinates can be expressed using Eq. (23), where x_i denotes the image coordinate, x_v the vehicle coordinate, K a camera-intrinsic function, R the rotation function, and T the camera movement function. When calibrating the AVM camera, the T matrix can be ignored. Thus, the T matrix is ignored in Eqs. (22), Eq. (23) is obtained as follows:

$$x_i = K[R|T]x_v = Hx_v. \tag{23}$$

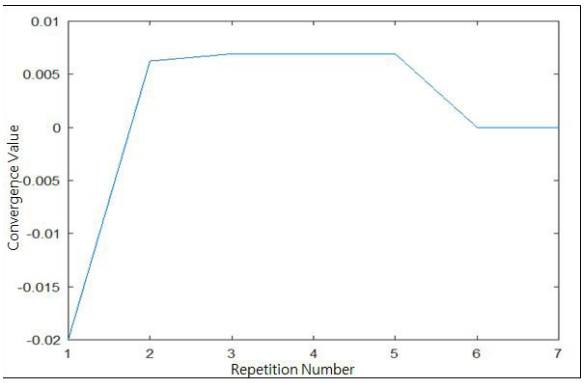

FIGURE 19. Repeated experimental results graph.

In Eq. (24), the R function is related to rotation, and the rotation about each axis is represented using Eq. (23).

$$R = R_x R_y R_z. \tag{24}$$

In Eq. (25), the AVM camera is calibrated by substituting the angle rotated about each axis. To find the optimal angle, the vanishing point approaches infinity, and it is repeatedly performed so that the two lines are parallel. The condition for the vanishing point approaching infinity is depicted in Eq. (25). Each point that appears in Fig. 18 should have the width of the actual parking line, W_G, and no difference should exist between the values of v_1 and v_3, and between the values of v_2 and v_4, in the y-axis coordinates. The rotation angle is calculated by repeatedly performing experiment until the condition for this is satisfied. One has

$$argmin(|W_G - W_R| + |W_G - W_L| + |v_1 - v_3| + |v_2 - v_4|). \tag{25}$$

Figure 19 depicts the results of the repeated experiment. In Fig. 19, the convergence is achieved after seven iterations.

IV. EXPERIMENTAL RESULTS

A. EXPERIMENTAL ENVIRONMENTS

Experiments were conducted at locations depicted similar to actual plant and service situations. The factory situation was tested in a garage and an underground parking lot depicted in Fig. 20. In the factory mode, the floor is coated and is the same as the garage floor. The underground parking lot was also constructed in an environment similar to the factory and garage, and thus the experiment could be conducted in a similar environment. As depicted in Fig. 20, the coated floor is often taped, and it is surrounded by various objects, which can interfere with recognition. Figure 20 (a) depicts the garage environment and Fig. 20 (b) illustrates the underground parking lot environment.

The cameras used in the experiment had a resolution of 1280 × 720. They were installed in the front, rear, left side, and right side of the vehicle. Figure 21 depicts the vehicle used for the test, which is Hyundai Genesis (4,990(L) × 1,890(W) × 1,480(H)) [25]. Fig. 22 depicts the camera installation.

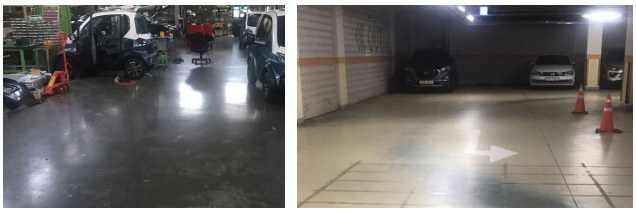

(a) (b)

FIGURE 20. Examples of experimental environments: (a) garage and (b) basement parking lot.

FIGURE 21. Test vehicle.

FIGURE 22. AVM camera installation.

To confirm the results for vehicles of various sizes, Sedan, sport utility vehicle (SUV), and micro-electric vehicles were used. The vehicles used are shown in Fig. 23; Figs. 23 (a) and 23 (b) show an SUV, Hyundai Santafe (4,190(L) × 1,880(W) × 1,690 (H)) [26], and a micro-electric vehicle, Cammsys CEVO-C (2,430(L) × 1,425(W) × 1,550 (H)) [27], respectively.

For the experiment, cameras were also installed on SUVs and micro-electric vehicles. Figures 24 (a) and 24 (b) show the installation on an SUV and micro-electric vehicle, respectively.

B. EXPERIMENTAL RESULTS FOR FACTORY-MODE CALIBRATION

In the factory mode, the camera was calibrated using the movement of the vehicle. To check the deviation in the calibration accuracy with respect to the position of the pattern, the experiment was performed with various pattern positions.

(a) (b)

FIGURE 23. Test vehicle: (a) SUV and (b) micro-electric vehicle.

(a) (b)

FIGURE 24. AVM camera installation: (a) SUV and (b) micro-electric vehicle.

FIGURE 25. Measurement distance error point.

TABLE 2. Repetition test result.

Mean Error	1.618 cm
Max. Error	6.211 cm
Min. Error	0.165 cm
Variance	1.820
Standard Deviation	1.349

The difference between the image position and actual position was measured, as depicted in Fig. 25. Hundred experiments were conducted to check repeatability by placing the vehicle at the same location and then measuring the error. Table 2 summarizes the results of the 100 experiments, and we confirm that the measurement error is less than 7 *cm*.

The experiment was conducted with a circular pattern, placed at a distance of 40 cm from the vehicle, using an SUV and micro-electric vehicle. Factory mode calibration was performed with each vehicle, and the actual distance

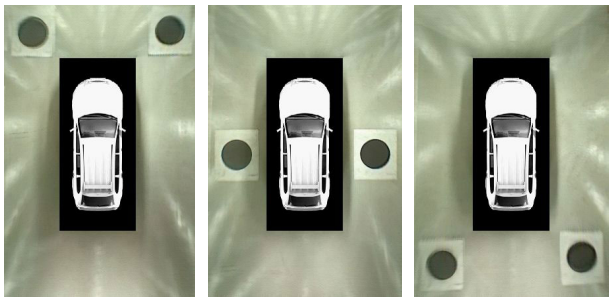

FIGURE 26. SUV test result images: (a) 12th frame, (b) 23th frame, and (c) 48th frame.

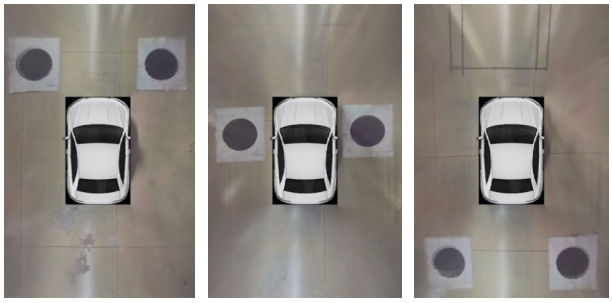

FIGURE 27. Micro-electric vehicle test result images:(a) 14th frame, (b) 31th frame, and (c) 49th frame.

from the selected point was measured, as shown in Fig. 25. An error of 1.7008 cm was observed in the case of SUV, and it was confirmed that calibration is required even if the camera position is raised from the ground owing to the height of the vehicle. Figure 26 depicts the results of the experiment for an SUV.

In the case of a micro-electric vehicle, an error of 0.837 cm was found in the size of the vehicle. Consequently, it was confirmed that the tolerance correction was required regardless of the size of the vehicle. Figure 27 shows the results of an experiment with a micro-electric vehicle.

Additional experiments were performed with respect to the distance between the vehicle and pattern, as depicted in Fig. 28.

Table 3 presents the results with respect to the distance between the vehicle and each pattern. It was confirmed that the error was less than 4 cm if the distance between the vehicle and pattern was equal to or less than 150 cm. However, when the distance is 160 and 170 cm, the error increases and becomes more than 6 cm, as depicted in Fig. 29. This implies that the circular pattern was wrongly extracted when the distance was equal to or more than 160 cm, while the extraction result is correct when the distance is equal to or less than 150 cm.

The experiments were conducted for the cases wherein the distance between the vehicle and the left and right circular patterns, respectively, was varied. The purpose of these experiments is to find that whether calibration could be

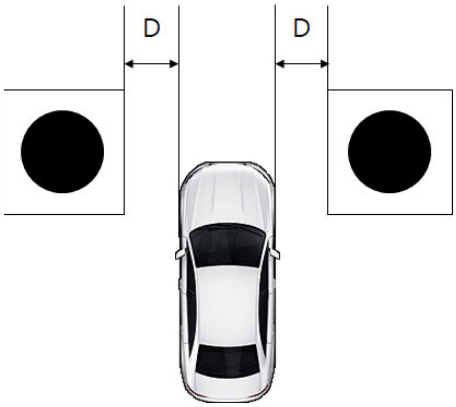

FIGURE 28. Circle-pattern-position testing method (equal distance between the vehicle and pattern in both the directions).

TABLE 3. Position-test result (equal distance between the vehicle and pattern in both directions).

Distance(cm)	Error (cm)	Distance (cm)	Error(cm)
20	0.5643	100	3.9772
30	3.1456	110	1.1591
40	3.8659	120	2.1149
50	2.8411	130	0.3076
60	2.6413	140	2.8935
70	2.584	150	1.2587
80	3.1231	160	7.3363
90	2.598	170	6.3884

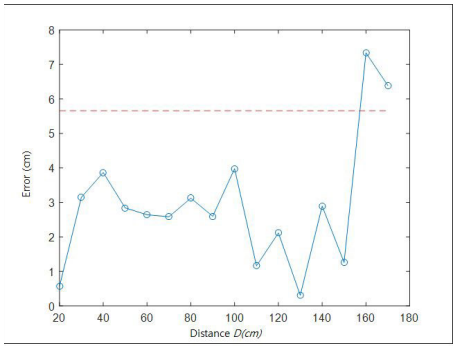

FIGURE 29. Position-testing-result graph (equal distance between the vehicle and pattern in both directions).

performed when the patterns were placed at different distances on the left and right sides of the vehicle. The experiment was performed by fixing one circular pattern at 20 *cm* and another at the distance of from the vehicle, as depicted in Fig. 30.

As shown in Table 4, when $D = 20\ cm$, the distance error is the same for the left and right circular patterns; however, when $D \geq 30\ cm$, a difference of distance error occurs between the left and right circular patterns. It was confirmed that calibration could be performed when $D \leq 140\ cm$, and it did not matter that the distance between the vehicle and

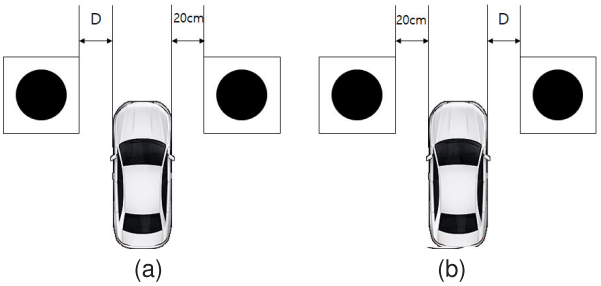

FIGURE 30. Circular-pattern-position testing method (one-way distance).(a) left circular pattern movement, and (b) right circular pattern movement.

TABLE 4. Position testing result (one-way distance).

Distance(cm)	Left Error (cm)	Right Error (cm)
20	1.8317	1.8317
30	1.1191	1.3645
40	0.2362	3.6984
50	1.2361	2.4633
60	0.5007	0.8013
70	0.7675	1.925
80	0.3113	2.2179
90	0.3292	1.6528
100	0.4822	2.2577
110	0.3523	1.0312
120	1.9257	3.5305
130	1.1197	4.8153
140	5.0012	6.1647

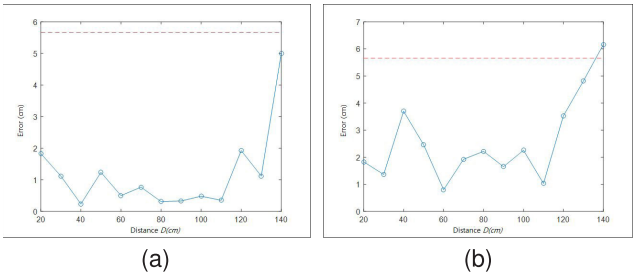

FIGURE 31. Position-testing-result graph (one-way distance): (a) left-distance-error graph and (b) right-distance-error graph.

the left and right circular patterns, respectively, was different. We achieved an error of less than 4 *cm* when $D \leq 120$ *cm*.

Figure 31 depicts a graph of the test results for the position of the circular pattern one-way distance. Fig. 31 (a) depicts the position error with respect to the distance between the left circular pattern and vehicle, and Fig. 31 (b) shows the position error with respect to the distance between the right circular pattern and vehicle.

Figure 32 depicts the experimental results with respect to the circular-pattern position. The results of the experiment are summarized in Tables 3 and 4. As depicted in Fig. 32, the calibration is performed irrespective of the left and right positions of the circular pattern. Fig. 32 (a) depicts the result

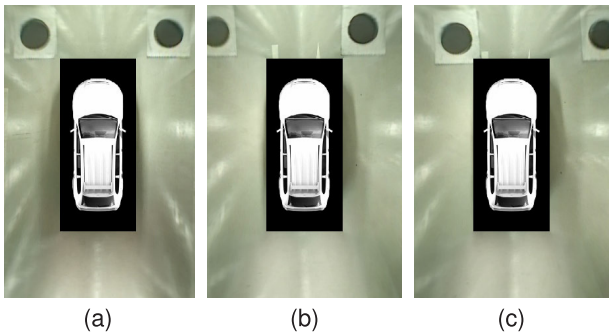

FIGURE 32. Calibration results for various pattern positions: (a) same distance, (b) rightward-movement result, and (c) leftward-movement result.

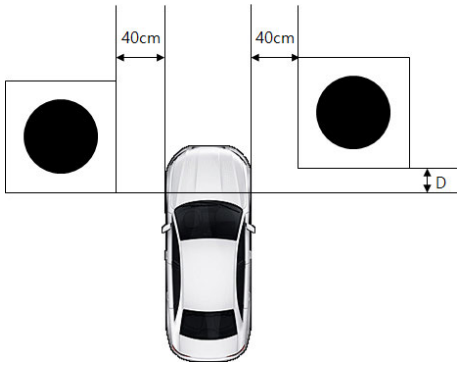

FIGURE 33. Circular-pattern-position testing method (inclination).

when the vehicle had passed through the exact center of the gap between the two circular patterns. Figure 32 (b) depicts the result when the vehicle had passed through the rightward side between the two circular patterns. Fig. 32 (c) depicts the result when the vehicle had passed through the leftward side between the two patterns. It is confirmed that the calibration was successfully performed even when the vehicle had not passed through the exact center of the gap between the patterns.

An experiment was also conducted when the line that connected the centers of both the patterns was not perpendicular to the moving direction of the vehicle, as depicted in Fig. 33.

As shown in Table 5, the tolerance correction was performed irrespective of the perpendicularity between the vehicle-movement direction and the line that connected the centers of both the patterns. When one of the patterns was located at equal to or more than 100 *cm* ahead of the other pattern, the calibration could not be performed because the pattern was not recognized. As depicted in Fig. 34, we achieved an error of less than 5.66 *cm* when the distance between both the patterns was equal to or less than 50 *cm*. Thus, AVM calibration could be performed when the angle between the vehicle-movement direction and the line that connected the centers of both the patterns was equal to or less than 12°.

Figure 35 depicts an image with a difference distance of 90 *cm*. Figure 35 (a) illustrates the front-camera image and Fig. 35 (b) the right-camera image. If the difference is more

TABLE 5. Position testing result (inclination).

Distance(cm)	Error (cm)	Distance (cm)	Error(cm)
0 (0°)	1.3837	50 (12°)	3.1539
10 (2°)	0.5489	60 (14°)	14.8319
20 (5°)	1.3933	70 (16°)	17.7376
30 (7°)	4.4372	80 (18°)	11.6157
40 (10°)	5.658	90 (20°)	12.7173

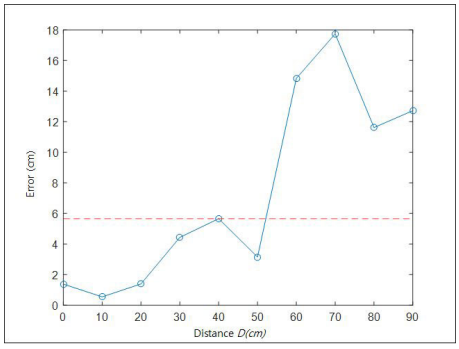

FIGURE 34. Position-testing-result graph (inclination).

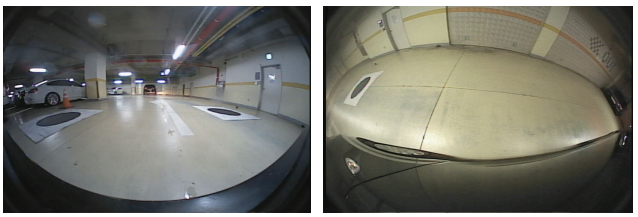

FIGURE 35. Pattern-position image at the same time: (a) front-camera image and (b) right-camera image.

than 100 *cm*, it is not recognized because of difference in the calibration pattern. As depicted in Fig. 35 (a), the circular pattern that is close to the camera appears large; however, the distant pattern may appear small and may not be recognized. Especially, in the case of the right-camera image depicted in Fig. 35 (b), the pattern is recognized because it lies at the image edge.

In Fig. 36, the result of the case wherein the position of the pattern is different is shown. As shown in Table 5, tolerance correction was performed even if there existed a distance difference between the two patterns. Experimental results in the factory mode show that when the vehicle and pattern are within a certain distance, the error is within 5.66 *cm*. When the distance to the pattern is within a certain range, the tolerance correction could be performed wherever the pattern is located on the left and right.

C. EXPERIMENTAL ENVIRONMENTS FOR SERVICE-MODE CALIBRATION

The service-mode experiments were performed using a parking-line image. For the experiment, the image obtained from the installed camera was rotated at a certain angle. In the experiment, the front, left and right camera images obtained

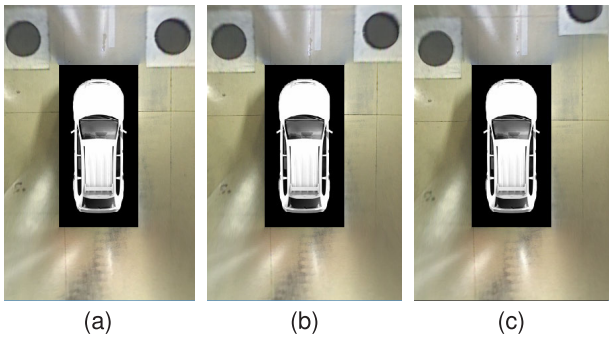

FIGURE 36. Calibration result for various pattern positions: (a) same distance, (b) distance difference: 20 cm, and (c) distance difference: 90 cm.

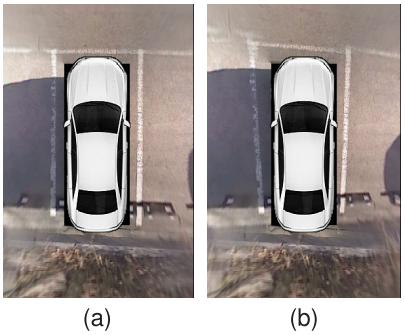

FIGURE 37. Rotated-image formation: (a) original image and (b) rotated image.

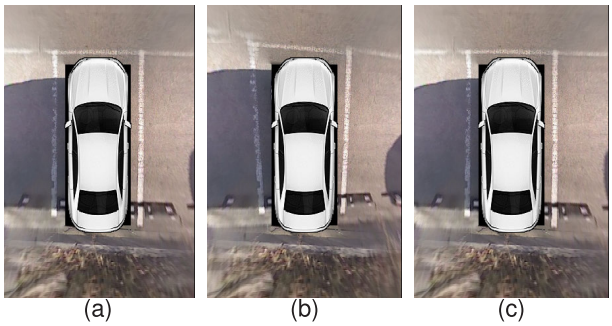

FIGURE 38. Rotated front camera calibration result: (a) original image, (b) rotated front camera image, and (c) correction result.

upon tilting the cameras by 0.8594° were used. Figure 37 depicts an AVM image as each camera is rotated. The front camera obtained the result of 0.8652° through 54 iterations, the left camera of 0.8537° through 78 iterations, and the right camera of 0.8537° through 89 iterations. Figure 38 depicts the result of compensating the rotation of the AVM camera. Figure 38 (a) shows the original image of the AVM. Fig. 38 (b) illustrates the camera-rotation result. Fig. 38 (c) depicts the rotation-compensation result. As depicted in Fig. 38, the rotated image was corrected using the calibration result based on the parking line.

Further, the method to use the lane markings during driving [13] was employed, and comparative experiments were performed. As it is impossible to compare the same image with method to use the lane markings during driving, the

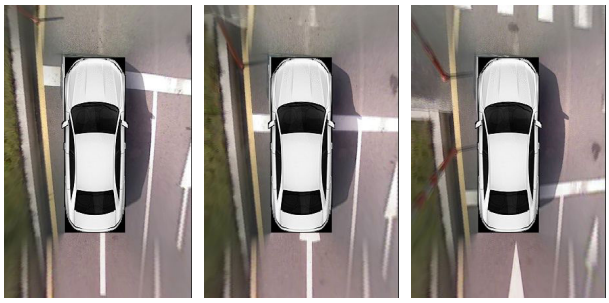

FIGURE 39. Examples of acquiring images to use lane markings during driving: (a) 289th frame, (b) 297th frame, and (c) 319th frame.

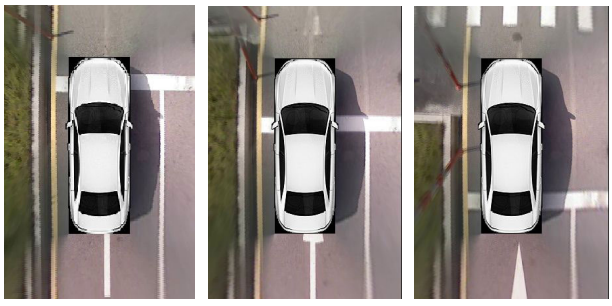

FIGURE 40. Examples of result images to use lane markings during driving: (a) 289th frame, (b) 297th frame, and (c) 319th frame.

TABLE 6. Comparison of test results.

Camera Position	Ground Truth	To Use Lane Markings[13]	Proposed Method
Front Camera	0.8594°	0.8480°	0.8652°
Left Camera	0.8594°	0.8422°	0.8537°
Right Camera	0.8594°	0.8652°	0.8537°

corrected values were compared for the cameras twisted at the same angle. The image acquired for the method to use the lane markings during driving is shown in Fig. 39. For the experiment, it was driven to acquire lane and stop line images.

Figure 40 shows the result of correcting the wrong position of the camera. It was confirmed that the wrongly positioned camera was corrected through the tolerance correction method while driving.

The comparison was conducted by acquiring driving images with a camera twisted at the same angle as the proposed method. When the three cameras were incorrectly positioned, the comparison was conducted, and the results shown in the Table 6 were obtained. As shown in Table 6, it was confirmed that tolerance correction performed was within 0.1719° for three cameras. In addition, it was verified that the proposed method has the same or higher performance as that of the method to use lane markings during driving using only the parking space and parking line. Consequently, it was confirmed that tolerance correction is possible within the service center without going outside.

In the service mode, calibration might not be performed when the parking line is not recognized. Experiments were

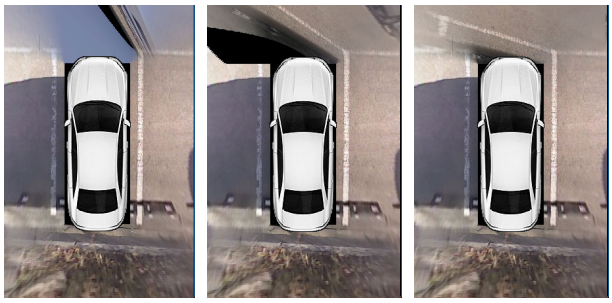

FIGURE 41. Front camera rotated by: (a) 11°, (b) 5°, and (c) 3°.

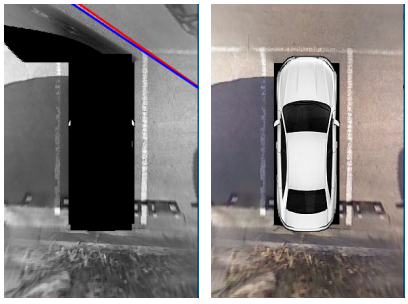

FIGURE 42. Rotated front camera correction result for Fig. 41(b): (a) parking-line-detection result and (b) correction result.

conducted with respect to which parking lines could be recognized. Figure 41 depicts the AVM image when the front camera was tilted. Figure 41 (a), (b), and (c) show the images obtained upon tilting the front camera by 11°, 5°, and 3°, respectively.

As depicted in Fig. 41, when the camera was tilted by 11°, the parking line was not visible and thus could not be recognized. However, when the camera was tilted by 5°, the parking line could be recognized, and thus service-mode calibration could be performed. Figure 42 depicts the results of parking-line recognition and calibration for the image in Fig. 41 (b). Furthermore, Fig. 42 (a) shows the result of parking-line recognition for the image in Fig. 41 (b). Figure 42 (b) shows the result of service-mode calibration performed using the parking-line-recognition result. Consequently, the camera-tilting angle of 5.72° was corrected to 5.517° through 21 iterations. For the side cameras, experiments were conducted when parking lines could be recognized. Figure 43 depicts the AVM image when the front camera is rotated. Figure 43 (a), (b), and (c) show the tilting of the right camera by 11°, 8.5°, and 5°, respectively.

As depicted in Fig. 43(a), when the camera was tilted by 11°, the parking line was not visible, and thus recognition was not possible. However, when the camera was tilted by 8.5°, the parking line could be recognized, and thus service-mode calibration could be performed. Figure 37 depicts the result of parking-line recognition and calibration for the image in Fig. 43 (b). Furthermore, Fig. 44 (a) shows the result of parking-line recognition for the image in Fig. 43 (b). Additionally, Fig. 44 (b) shows the result of

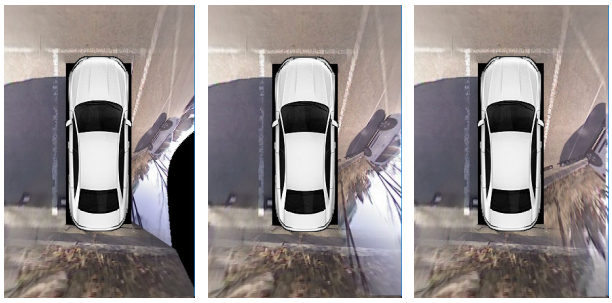

FIGURE 43. Rotated right camera: (a) 11°, (b) 8.5°, and (c) 5°.

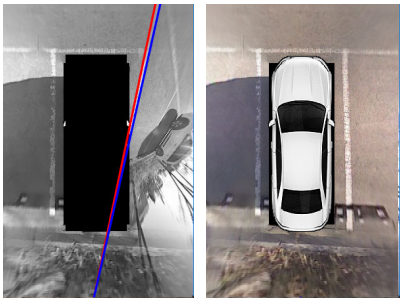

FIGURE 44. Rotated right camera calibration result for Fig. 43(b): (a) parking-line-detection result and (b) correction result.

service-mode calibration performed using the parking-line-recognition result. Consequently, the camera-tilting angle of 8.59° was corrected to 8.68° through 27 iterations.

V. CONCLUSION

We proposed an automatic AVM-camera-calibration method. The shipping method was defined as factory mode and the recalibration method as service mode, so that calibration could be performed for various cases. In the factory mode, calibration was performed when there was no camera-mounting information; a vehicle was passed between two circular patterns to calibrate AVM cameras to synthesize top-view images. When the vehicle passed between two circular patterns, both of them were recognized in each frame. The proposed method determined whether the recognized circular patterns could be used for camera calibration. The AVM camera were calibrated using two circular patterns in the video. As a result of calibrating the AVM camera by using the vehicle-motion information and circular patterns, we achieved an error within 5.66 cm. The service mode corrects the camera distortion due to internal and external influences. For the distortion correction, the service mode recognized the parking line, calculated the angle of the parking line, and corrected the AVM-camera-calibration results. As a result of the correction using the parking line, the correction was made within 0.1°. The proposed method achieved automatic AVM-camera calibration in two modes, respectively. In future, we will study how to perform calibration faster with fewer computations and increase calibration accuracy.

REFERENCES

[1] C.-H. Kum, D.-C. Cho, M.-S. Ra, and W.-Y. Kim, "Lane detection system with around view monitoring for intelligent vehicle," in *Proc. Int. SoC Design Conf. (ISOCC)*, Busan, South Korea, Nov. 2013, pp. 215–218.

[2] Y. C. Liu, K. Y. Lin, and Y. S. Chen, "Bird's-eye view vision system for vehicle surrounding monitoring," in *Proc. Int. Workshop Robot Vis.*, Auckland, New Zealand, Feb. 2008, pp. 207–218.

[3] M. M. Trivedi, T. Gandhi, and J. McCall, "Looking-in and looking-out of a vehicle: Computer-vision-based enhanced vehicle safety," *IEEE Trans. Intell. Transp. Syst.*, vol. 8, no. 1, pp. 108–120, Mar. 2007.

[4] H. G. Jung, D. S. Kim, P. J. Yoon, and J. Kim, "Parking slot markings recognition for automatic parking assist system," in *Proc. IEEE Intell. Vehicles Symp.*, Tokyo, Japan, Jun. 2006, pp. 106–113.

[5] Y. Lee and S. Chang, "Development of a verification method on ultrasonic-based perpendicular parking assist system," in *Proc. 18th IEEE Int. Symp. Consum. Electron.*, Jeju, South Korea, Jun. 2014, pp. 1–3.

[6] H. Satonaka, M. Okuda, S. Hayasaka, T. Endo, Y. Tanaka, and T. Yoshida, "Development of parking space detection using an ultrasonic sensor," in *Proc. 13th ITS World Congr.*, London, U.K., Oct. 2006, pp. 1–10.

[7] S. Li and Y. Hai, "Easy calibration of a blind-spot-free fisheye camera system using a scene of a parking space," *IEEE Trans. Intell. Transp. Syst.*, vol. 12, no. 1, pp. 232–242, Mar. 2011.

[8] J. Pyo, S. Hyun, and Y. Jeong, "Auto-image calibration for AVM system," in *Proc. Int. SoC Design Conf.*, Gyungju, South Korea, Nov. 2015, pp. 307–308.

[9] J. Bang, J. Pyo, and Y. Jeong, "Automatic image deviation detection for AVM auto-calibration," in *Proc. Int. SoC Design Conf.*, Jeju, South Korea, Oct. 2016, pp. 159–160.

[10] Y. L. Chang, L. Y. Hsu, and O. T. C. Chen, "Auto-calibration around-view monitoring system," in *Proc. IEEE Veh. Technol. Conf.*, Las Vegas, NV, USA, Sep. 2013, pp. 1–5.

[11] K. Natroshvili and K. U. Scholl, "Automatic extrinsic calibration methods for surround view systems," in *Proc. IEEE Intell. Vehicles Symp.*, Redondo Beach, CA, USA, Jun. 2017, pp. 82–88.

[12] C.-C. Lin and M.-S. Wang, "A vision based top-view transformation model for a vehicle parking assistant," *Sensors*, vol. 12, no. 4, pp. 4431–4446, Mar. 2012.

[13] K. Choi, H. Jung, and J. Suhr, "Automatic calibration of an around view monitor system exploiting lane markings," *Sensors*, vol. 18, no. 9, p. 2956, Sep. 2018.

[14] Y. Ishii, K. Asari, H. Hongo, and H. Kano, "A practical calibration method for top view image generation," in *Dig. Tech. Papers-Int. Conf. Consum. Electron.*, Sep. 2008, pp. 1–2.

[15] L. Xu, E. Oja, and P. Kultanen, "A new curve detection method: Randomized Hough transform (RHT)," *Pattern Recognit. Lett.*, vol. 11, no. 5, pp. 331–338, May 1990.

[16] K. Hahn, Y. Han, and H. Hahn, "Ellipse detection using a randomized Hough transform based on edge segment merging scheme," in *Proc. 6th WSEAS Int. Conf. Signal Process., Robot. Autom.*, Feb. 2007, pp. 1–6.

[17] S. Sharma and U. R. Nitasha, "Ellipse detection using canny edge detection algorithm," *Int. J. Comput. Appl. Inf. Technol.*, vol. 1, pp. 45–47, Sep. 2012.

[18] A. A. Rad, K. Faez, and N. Qaragozlou, "Fast circle detection using gradient pair vectors," in *Proc. 7th Digit. Image Comput. Techn. Appl.*, Dec. 2003, pp. 879–888.

[19] D.-J. Kang and W.-H. Lee, "Automatic circle pattern extraction and camera calibration using fast adaptive binarization and plane homography," *Int. J. Precis. Eng. Manuf.*, vol. 11, no. 1, pp. 13–21, Feb. 2010.

[20] J. Kannala, M. Salo, and J. Heikkilä, "Algorithms for Computing a planar homography from Conics in Correspondence," in *Proc. 17th BMVC*, Sep. 2006, pp. 77–86.

[21] H. H. S. Ip and Y. Chen, "Planar rectification by solving the intersection of two circles under 2D homography," *Pattern Recognit.*, vol. 38, no. 7, pp. 1117–1120, Jul. 2005.

[22] O. Chum and J. Matas, "Homography estimation from correspondences of local elliptical features," in *Proc. 21st Int. Conf. Pattern Recognit.*, Tsukuba, Japan, Nov. 2012, pp. 3236–3239.

[23] M. I. A. Lourakis, "Plane metric rectification from a single view of multiple coplanar circles," in *Proc. 16th IEEE Int. Conf. Image Process.*, Cairo, Egypt, Nov. 2009, pp. 509–512.

[24] L. Peng, Z. Jianwei, G. Konghui, and Z. Hu, "A parking-line detection method based on edge direction," in *Proc. IEEE Int. Conf. Secur., Pattern Anal., Cybern.*, Wuhan, China, Oct. 2014, pp. 105–108.

[25] Hyundai Motor Company. (Oct. 23, 2015). *Genesis DH Vehicle Information*. Accessed: Sep. 17, 2020. [Online]. Available: https://www.genesis.com/kr/ko/support/download-center/genesis-models.html
[26] Hyundai Motor Company. (May 2, 2018). *Santafe DM Vehicle Information*. Accessed: Sep. 23, 2020. [Online]. Available: https://www.hyundai.com/kr/ko/download-center.html
[27] Cammsys Corp. (Jul. 1, 2019). *CEVO-C*. Accessed: Sep. 24, 2020. [Online]. Available: https://www.cevo.co.kr

YUN HEE LEE received the B.S. and M.S. degrees in electronic engineering from Sogang University, Seoul, South Korea, in 2003 and 2005, respectively. He is currently pursuing the Ph.D. degree in electronics and computer engineering with Hanyang University, Seoul. From January 2005 to January 2016, he was with the Global Research and Development H.Q., MANDO Corporation, South Korea, where he developed environmental recognition systems for driver assistant systems. From January 2016 to July 2020, he was with Cammsys, Incheon, South Korea. Since 2020, he has been with Litbig, Seongnam, Gyeonggi, South Korea. His research interests include driver-assistant systems and automotive vision.

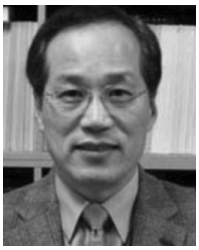

WHOI-YUL KIM (Member, IEEE) received the Ph.D. degree in electrical engineering from Purdue University, West Lafayette, IN, USA, in 1989. From 1989 to 1994, he was an Assistant Professor with The University of Texas at Dallas. He joined Hanyang University, in 1994, where he is currently a Professor with the Department of Electronic Engineering. His research interests include health monitoring using computer vision, intelligent surveillance, machine vision, advanced driver assistance systems, and 3-D vision systems in sports.